

1 **Herd immunity thresholds for SARS-CoV-2 estimated from** 2 **unfolding epidemics**

3 Ricardo Aguas^{1†}, Rodrigo M. Corder^{2†}, Jessica G. King³, Guilherme Gonçalves⁴,
4 Marcelo U. Ferreira², M. Gabriela M. Gomes^{5,6*}

5 ¹ *Centre for Tropical Medicine and Global Health, Nuffield Department of Medicine,*
6 *University of Oxford, Oxford, United Kingdom.*

7 ² *Instituto de Ciências Biomédicas, Universidade de São Paulo, São Paulo, Brazil.*

8 ³ *Institute of Evolutionary Biology, University of Edinburgh, Edinburgh, United*
9 *Kingdom.*

10 ⁴ *Unidade Multidisciplinar de Investigação Biomédica, Instituto de Ciências*
11 *Biomédicas Abel Salazar, Universidade do Porto, Porto, Portugal.*

12 ⁵ *Department of Mathematics and Statistics, University of Strathclyde, Glasgow,*
13 *United Kingdom.*

14 ⁶ *Centro de Matemática da Universidade do Porto, Porto, Portugal.*

15

16 † These authors contributed equally to this work.

17 * Correspondence and requests for materials should be addressed to M.G.M.G. (email:
18 gabriela.gomes@strath.ac.uk).

19 **As severe acute respiratory syndrome coronavirus 2 (SARS-CoV-2) spreads, the**
20 **susceptible subpopulation declines causing the rate at which new infections occur**
21 **to slow down. Variation in individual susceptibility or exposure to infection**
22 **exacerbates this effect. Individuals that are more susceptible or more exposed**
23 **tend to be infected and removed from the susceptible subpopulation earlier. This**
24 **selective depletion of susceptibles intensifies the deceleration in incidence.**
25 **Eventually, susceptible numbers become low enough to prevent epidemic growth**
26 **or, in other words, the herd immunity threshold is reached. Here we fit**
27 **epidemiological models with inbuilt distributions of susceptibility or exposure to**
28 **SARS-CoV-2 outbreaks to estimate basic reproduction numbers (R_0) alongside**
29 **coefficients of individual variation (CV) and the effects of containment strategies.**
30 **Herd immunity thresholds are then calculated as $1 - (1/R_0)^{1/(1+CV^2)}$ or $1 -$**
31 **$(1/R_0)^{1/(1+2CV^2)}$, depending on whether variation is on susceptibility or**
32 **exposure. Our inferences result in herd immunity thresholds around 10-20%,**
33 **considerably lower than the minimum coverage needed to interrupt transmission**
34 **by random vaccination, which for R_0 higher than 2.5 is estimated above 60%.**
35 **We emphasize that the classical formula, $1 - 1/R_0$, remains applicable to**
36 **describe herd immunity thresholds for random vaccination, but not for**
37 **immunity induced by infection which is naturally selective. These findings have**
38 **profound consequences for the governance of the current pandemic given that**
39 **some populations may be close to achieving herd immunity despite being under**
40 **more or less strict social distancing measures.**

41 Scientists throughout the world have engaged with governments, health agencies, and
42 with each other, to address the ongoing pandemic of coronavirus disease (COVID-
43 19). Mathematical models have been central to important decisions concerning

44 contact tracing, quarantine, and social distancing, to mitigate or suppress the initial
45 pandemic spread¹. Successful suppression, however, may leave populations at risk to
46 resurgent waves due to insufficient acquisition of immunity. Models have thus also
47 addressed longer term SARS-CoV-2 transmission scenarios and the requirements for
48 continued adequate response². This is especially timely as countries relax lockdown
49 measures that have been in place over recent months with varying levels of success in
50 tackling national outbreaks.

51 Here we demonstrate that individual variation in susceptibility or exposure
52 (connectivity) accelerates the acquisition of immunity in populations. More
53 susceptible and more connected individuals have a higher propensity to be infected
54 and thus are likely to become immune earlier. Due to this selective immunization by
55 natural infection, heterogeneous populations require less infections to cross their herd
56 immunity threshold (HIT) than suggested by models that do not fully account for
57 variation. We integrate continuous distributions of susceptibility or connectivity in
58 otherwise basic epidemic models for COVID-19 which account for realistic
59 intervention effects and show that as coefficients of variation (CV) increase from 0 to
60 5, HIT declines from over 60%^{3,4} to less than 10%. We then fit these models to series
61 of daily new cases to estimate CV alongside basic reproduction numbers (R_0) and
62 derive the corresponding HITs.

63 **Effects of individual variation on SARS-CoV-2 transmission**

64 SARS-CoV-2 is transmitted primarily by respiratory droplets and modelled as a
65 susceptible-exposed-infectious-recovered (SEIR) process.

66 *Variation in susceptibility to infection*

67 Individual variation in susceptibility is integrated as a continuously distributed factor
68 that multiplies the force of infection upon individuals⁵ as

$$69 \quad \dot{S}(x) = -\lambda(x)xS(x), \quad (1)$$

$$70 \quad \dot{E}(x) = \lambda(x)x[S(x) + \sigma R(x)] - \delta E(x), \quad (2)$$

$$71 \quad \dot{I}(x) = \delta E(x) - \gamma I(x), \quad (3)$$

$$72 \quad \dot{R}(x) = (1 - \phi)\gamma I(x) - \sigma\lambda(x)xR(x), \quad (4)$$

73 where $S(x)$ is the number of individuals with susceptibility x , $E(x)$ and $I(x)$ are the
74 numbers of individuals who originally had susceptibility x and became exposed and
75 infectious, while $R(x)$ counts those who have recovered and have their susceptibility
76 reduced to a reinfection factor σ due to acquired immunity. δ is the rate of
77 progression from exposed to infectious, γ is the rate of recovery or death, ϕ is the
78 proportion of individuals who die as a result of infection and $\lambda(x) =$
79 $(\beta/N) \int [\rho E(y) + I(y)] dy$ is the average force of infection upon susceptible
80 individuals in a population of size N and transmission coefficient β . Standardizing so
81 that susceptibility distributions have mean $\int xg(x) dx = 1$, given a probability
82 density function $g(x)$, the basic reproduction number is

$$83 \quad R_0 = \beta \left(\frac{\rho}{\delta} + \frac{1}{\gamma} \right), \quad (5)$$

84 where ρ is a factor measuring the infectivity of individuals in compartment E in
85 relation to those in I . The coefficient of variation in individual susceptibility $CV =$
86 $\sqrt{\int (x-1)^2 g(x) dx}$ is explored as a parameter. Non-pharmaceutical interventions
87 (NPIs) designed to control transmission typically reduce β and hence R_0 . We denote
88 the resulting controlled reproduction number by R_c . The effective reproduction

89 number R_{eff} is another useful indicator obtained by multiplying R_c by the
90 susceptibility of the population, in this case written as $R_{eff}(t) =$
91 $R_c(t) \int xS(x, t) dx/N(t)$ to emphasize its time dependence.

92 Figure 1 depicts model trajectories fitted to suppressed epidemics (orange) in 4
93 European countries (Belgium, England, Portugal and Spain) assuming gamma
94 distributed susceptibility and no reinfection ($\sigma = 0$). We estimate: R_0 rounding 5
95 (Belgium), 2.9 (England), 4.3 (Portugal) and 4.1 (Spain); individual susceptibility CV
96 reaching 3.9 (Belgium), 1.9 (England), 4.3 (Portugal) and 3.2 (Spain); and overall
97 intervention efficacy at maximum (typically during lockdown) being 60% (Belgium),
98 48% (England), 69% (Portugal) and 63% (Spain). Another estimated parameter is the
99 day when NPIs begin to affect transmission, after which we assume a linear
100 intensification from baseline over 21 days, remaining at maximum intensity for 30
101 days and linearly lifting back to baseline over a period of 120 days (although we have
102 confirmed that the results do not change significantly if measures are lifted over
103 slightly longer time frames, such as 150 or 180 days). Denoting by $d(t)$ the
104 proportional reduction in average risk of infection due to interventions, in this case we
105 obtain $R_c(t) = [1 - d(t)]R_0$ which is depicted for each country, alongside $R_{eff}(t)$,
106 underneath the respective epidemic trajectories. Overlaid on the R_c plots are mobility
107 data from Google⁶, showing excellent agreement with our independently chosen
108 framework and estimate for the time R_{eff} starts declining. To assess the potential for
109 case numbers to overshoot if NPIs had not been applied, we rerun the model with
110 $d(t) = 0$ and obtain the unmitigated epidemics (black). Further details and sensitivity
111 analyses are described in Methods.

112 *Variation in connectivity*

113 In a directly transmitted infectious disease, such as COVID-19, variation in exposure
114 to infection is primarily governed by patterns of connectivity among individuals. We
115 incorporate this in the system (Equations 1-4) assuming that individuals mix at
116 random (but see Methods for more general formulations that enable other mixing
117 patterns). Under random mixing and heterogeneous connectivity, the force of
118 infection⁷ is written as $\lambda(x) = (\beta/N)(\int y[\rho E(y) + I(y)] dy / \int yg(y) dy)$, the basic
119 reproduction number is

$$120 \quad R_0 = (1 + CV^2)\beta \left(\frac{\rho}{\delta} + \frac{1}{\gamma} \right), \quad (6)$$

121 $R_c(t)$ is as above and $R_{eff}(t)$ is derived by a more general expression given in
122 Methods. Applying this model to the same epidemics as before we estimate: R_0
123 rounding 7.1 (Belgium), 3.8 (England), 7.9 (Portugal) and 6.6 (Spain); individual
124 susceptibility CV reaching 2.9 (Belgium), 1.6 (England), 4.0 (Portugal) and 2.7
125 (Spain); and intervention efficacy during lockdown being 73% (Belgium), 58%
126 (England), 80% (Portugal) and 72% (Spain).

127 Comparing the two models, variation in connectivity systematically leads to estimates
128 that are higher for R_0 , lower for CV, and higher for the efficacy of non-
129 pharmaceutical interventions. Nevertheless, the percentage of the population required
130 to be immune to curb the epidemic and prevent future waves when interventions are
131 lifted appears remarkably conserved across models: 9.6 vs 11% (Belgium); 20 vs 21%
132 (England); 7.3 vs 6.0% (Portugal); and 12 vs 11% (Spain). This property is further
133 explored below.

134 **Herd immunity thresholds and their conserveness across models**

135 Individual variation in risk of acquiring infection is under selection by the force of
136 infection, whether individual differences are due to biological susceptibility,
137 exposure, or both. The most susceptible or exposed individuals are selectively
138 removed from the susceptible pool as they become infected and eventually recover
139 (some die), resulting in decelerated epidemic growth and accelerated induction of
140 immunity in the population. In essence, the *herd immunity threshold* defines the
141 percentage of the population that needs to be immune to reverse epidemic growth and
142 prevent future waves. When individual susceptibility or connectivity is gamma-
143 distributed and mixing is random, HIT curves can be derived analytically⁸ from the
144 model systems (Equations 1-4, with the respective forces of infections). In the case of
145 variation in susceptibility to infection we obtain

$$146 \quad HIT = 1 - \left[\frac{1 - \sigma R_0}{(1 - \sigma)R_0} \right]^{\frac{1}{1+CV^2}}, \quad (7)$$

147 while variable connectivity results in

$$148 \quad HIT = 1 - \left[\frac{1 - \sigma R_0}{(1 - \sigma)R_0} \right]^{\frac{1}{1+2CV^2}}. \quad (8)$$

149 In more complex cases HIT curves can be approximated numerically. Figure 3 shows
150 the expected downward trends in HIT and the sizes of the respective unmitigated
151 epidemics for SARS-CoV-2 without reinfection ($\sigma = 0$) as the coefficients of
152 variation are increased (gamma distribution shapes adopted here are illustrated in
153 Extended Data Figure 1; for robustness of the trends to other distributions see Gomes
154 et al⁹). Values of R_0 and CV estimated for our study countries are overlaid to mark
155 the respective HIT and final epidemic sizes. While herd immunity is expected to
156 require 60-80% of a homogeneous population to have been infected, at the cost of

157 infecting almost the entire population if left unmitigated, given an R_0 between 2.5 and
158 5, these percentages drop to the range 10-20% or lower when CV is roughly between
159 2 and 5.

160 When acquired immunity is not 100% effective ($\sigma > 0$) HITs are relatively higher
161 (Extended Data Figure 2). However, there is an upper bound for how much it is
162 reasonable to increase σ before the system enters a qualitatively different regime.

163 Above $\sigma = 1/R_0$ – the *reinfection threshold*^{10,11}– infection becomes stably endemic
164 and the HIT concept no longer applies. Respiratory viruses are typically associated
165 with epidemic dynamics below the reinfection threshold, characterized by seasonal
166 epidemics intertwined with periods of undetection.

167 Individual variation in exposure, in contrast with susceptibility, accrues from complex
168 patterns of human behaviour which have been simplified in our model. To explore the
169 scope of our results we generalise our models (Methods) by relaxing some key
170 assumptions. First, we enable mixing to be assortative in the sense that individuals
171 contact predominantly with those of similar connectivity. Formally, an individual
172 with connectivity x , rather than being exposed uniformly to individuals of all
173 connectivities y , has contact preferences described by a normal distribution on the
174 difference $y - x$. We find this modification to have negligible effect on HIT
175 (Extended Data Figure 3). Second, we allow connectivity distributions to change in
176 shape (not only scale) when subject to social distancing. In particular we modify the
177 model so that CV reduces in proportion to the intensity of social distancing (Extended
178 Data Figure 4) and replicate the fittings to epidemics in our study countries (Extended
179 Data Figure 5). We find a general tendency for this model to estimate higher values
180 for R_0 and CV while HIT remains again remarkably robust to the change in model

181 assumptions.

182 **Herd immunity thresholds and seroprevalence at sub-national levels**

183 As countries are conducting immunological surveys to assess the extent of exposure
184 to SARS-CoV-2 in populations it is of practical importance to understand how HIT
185 may vary across regions. We have redesigned our analyses to address this question.
186 Series of daily new cases were stratified by region. Fitting the models simultaneously
187 to the multiple series enabled the estimation of local parameters (R_0 and CV) while
188 the effects of NPIs were estimated at country level. Extended Data Figures 6-9 show
189 how the modelled epidemics fit the regional data and include an additional metric to
190 describe the cumulative infected percentage. These model projections are comparable
191 to data from seroprevalence studies such as Spain¹². We emphasise that
192 seroprevalence estimates generally lie slightly below our cumulative infection curves
193 (Extended Data Figure 9) consistently with recent findings that a substantial fraction
194 of infected individual does not exhibit detectable antibodies¹³. In addition to their
195 practical utility these results begin to unpack some of the variation in HIT within
196 countries: Belgium (9.4-11%), England (16-26%), Portugal (7.1-9.9%) and Spain
197 (7.5-21%).

198 **Discussion**

199 The concept of *herd immunity* was developed in the context of vaccination
200 programs^{14,15}. Defining the percentage of the population that must be immune to
201 cause infection incidences to decline, HITs constitute useful targets for vaccination
202 coverage. In idealized scenarios of vaccines delivered at random and individuals
203 mixing at random, HITs are given by a simple formula ($1 - 1/R_0$) which, in the case
204 of SARS-CoV-2, suggests that 60-80% of randomly chosen subjects of the population

205 would need be immunized to halt spread considering estimates of R_0 between 2.5 and
206 5. This formula does not apply to infection-induced immunity because natural
207 infection does not occur at random. Individuals who are more susceptible or more
208 exposed are more prone to be infected and become immune, providing greater
209 community protection than random vaccination¹⁶. In our model, the HIT declines
210 sharply when coefficients of variation increase from 0 to 2 and remains below 20%
211 for more variable populations. The magnitude of the decline depends on what
212 property is heterogeneous and how it is distributed among individuals, but the
213 downward trend is robust as long as susceptibility or exposure to infection are
214 variable (Figure 3 and Extended Data Figures 3) and acquired immunity is efficacious
215 enough to keep transmission below the reinfection threshold (Extended Data Figure
216 2).

217 Several candidate vaccines against SARS-CoV-2 are showing promising safety and
218 immunogenicity in early-phase clinical trials^{17,18}, although it is not yet known how
219 this will translate into effective protection. We note that the reinfection threshold^{10,11}
220 informs not only the requirements on naturally acquired immunity but, similarly, it
221 sets a target for how efficacious a vaccine needs to be in order to effectively interrupt
222 transmission. Specifically, given an estimated value of R_0 we should aim for a
223 vaccine efficacy of $1 - 1/R_0$ (60% or 80% if R_0 is 2.5 or 5, respectively). A vaccine
224 whose efficacy is insufficient to bring the system below the reinfection threshold will
225 not interrupt transmission.

226 Heterogeneity in the transmission of respiratory infections has traditionally focused
227 on variation in exposure summarized into age-structured contact matrices. Besides
228 overlooking differences in susceptibility given exposure, the aggregation of

229 individuals into age groups reduces coefficients of variation. We calculated CV for
230 the landmark POLYMOD matrices^{19,20} and obtained values between 0.3 and 0.5.
231 Recent studies of COVID-19 integrated contact matrices with age-specific
232 susceptibility to infection (structured in three levels)²¹ or with social activity (three
233 levels also)²² which, again, resulted in coefficients of variation less than unity. We
234 show that models with coefficients of variation of this magnitude would appear to
235 differ only moderately from homogeneous approximations when compared with our
236 estimates, which are consistently above 1 in England and above 2 in Belgium,
237 Portugal and Spain. In contrast with reductionistic procedures that aim to reconstruct
238 variation from correlate markers left on individuals (such as antibody or reactive T
239 cells for susceptibility, or contact frequencies for exposure), we have embarked on a
240 holistic approach designed to infer the whole extent of individual variation from the
241 imprint it leaves on epidemic trajectories. Our estimates are therefore expected to be
242 higher and should ultimately be confronted with more direct measurements as these
243 become available. Adam et al²³ conducted a contact tracing study in Hong Kong and
244 estimated a coefficient of variation of 2.5 for the number of secondary infections
245 caused by individuals, attributing 80% of transmission to 20% of cases. This
246 statistical dispersion has been interpreted as reflecting a common pattern of contact
247 heterogeneity which has been corroborated by studies that specifically measure
248 mobility²⁴. According to our inferences, 20% of individuals may be responsible for
249 47-94% infections depending on model and country. In parallel, there is accumulating
250 evidence of individual variation in the immune system's ability to control SARS-
251 CoV-2 infection following exposure^{25,26}. While our inferences serve their purpose of
252 improving accuracy in model predictions, diverse studies such as these are necessary
253 for developing interventions targeting individuals who may be at higher risk of being

254 infected and propagating infection in the community.

255 Country-level estimates of R_0 reported here are in the range 3-5 when individual
256 variation in susceptibility is factored and 4-8 when accounting for variation in
257 connectivity. The homogeneous version of our models would have estimated R_0
258 between 2.4 and 3.3, in line with other studies²⁷. Estimates for England suggest lower
259 baseline R_0 and lower CV in comparison with the other study countries (Belgium,
260 Portugal and Spain). The net effect is a slightly higher HIT in England which
261 nevertheless we estimate around 20%. The lowest HIT, at less than 10%, is estimated
262 in Portugal, with higher R_0 and higher CV. NPIs reveal less impact under variable
263 susceptibility (48-69%), followed by variable connectivity (58-80%), and finally
264 appear to inflate and agree with Flaxman et al²⁷ when homogeneity assumptions are
265 made (65-89%), although this does not affect the HIT which relates to pre-pandemic
266 societies.

267 More informative than reading these numbers, however, is to look at simulated
268 projections for daily new cases over future months (Figures 1 and 2). In all four
269 countries considered here we foresee HIT being achieved between July and October
270 and the COVID-19 epidemic being mostly resolved by the end of 2020. Looking
271 back, we conclude that NPIs had a crucial role in halting the growth of the initial
272 wave between February and April. Although the most extreme lockdown strategies
273 may not be sustainable for longer than a month or two, they proved effective at
274 preventing overshoot, keeping cases within health system capacities, and may have
275 done so without impairing the development of herd immunity.

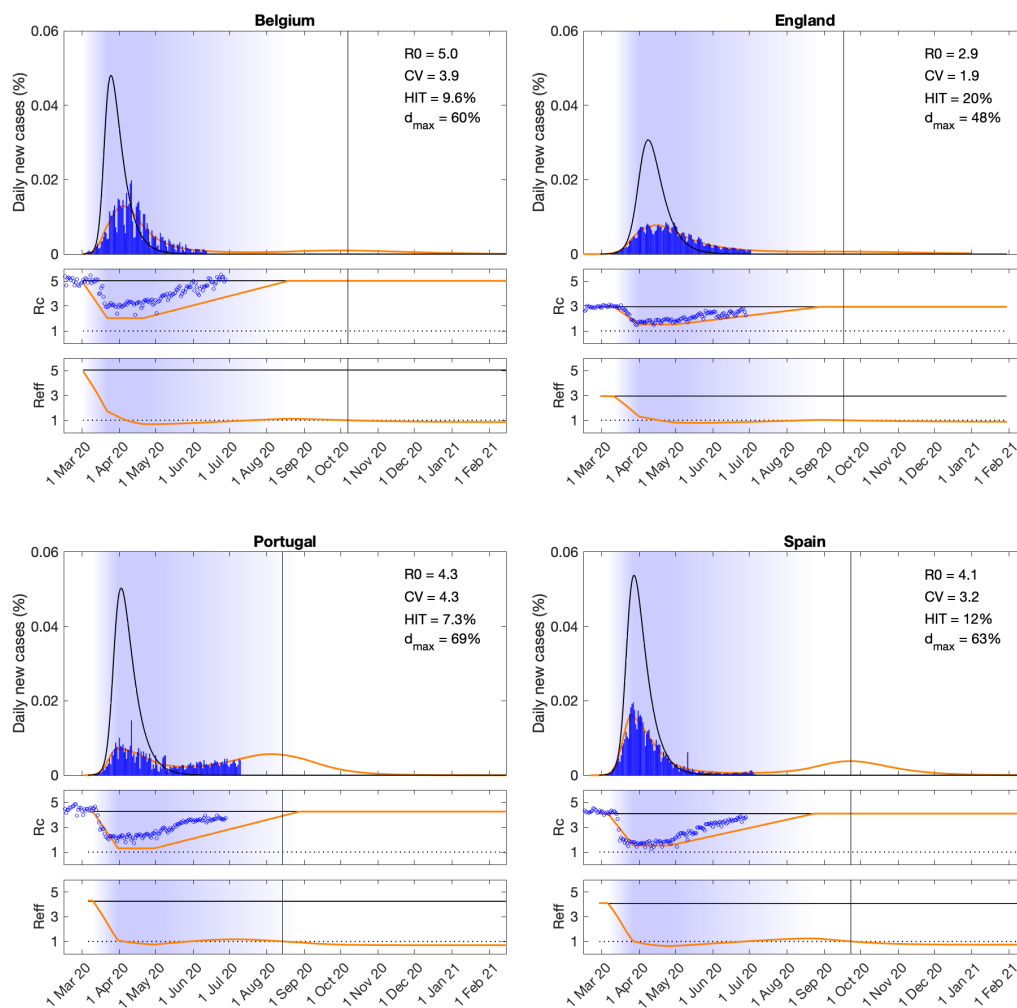
276

- 277 1. Ferguson, N. M., et al. Impact of non-pharmaceutical interventions (NPIs) to reduce
278 COVID-19 mortality and healthcare demand (Imperial College COVID-19 Response
279 Team, 2020). 10.25561/77482.
- 280 2. Kissler, S. M., Tedijanto, C., Goldstein, E., Grad, Y. H. & Lipsitch, M. Projecting the
281 transmission dynamics of SARS-CoV-2 through the postpandemic period. *Science* **368**,
282 860-868 (2020).
- 283 3. Wu, J. T., Leung, K. & Leung, G. M. Nowcasting and forecasting the potential domestic
284 and international spread of the 2019-nCoV outbreak originating in Wuhan, China: a
285 modelling study. *Lancet* **395**, 689-697 (2020).
- 286 4. Kwok, K. O., Lai, F., Wei, W. I., Wong, S. Y. S. & Tang, J. Herd immunity – estimating
287 the level required to halt the COVID-19 epidemics in affected countries. *J. Infect.* **80**,
288 e32-e33 (2020).
- 289 5. Diekmann, O., Heesterbeek, J. A. P. & Metz, J. A. J. On the definition and computation
290 of the basic reproduction ratio R_0 in models for infectious diseases in heterogeneous
291 populations. *J. Math. Biol.* **28**, 365-382 (1990).
- 292 6. Google, COVID-19 Community Mobility Reports (2020).
- 293 7. Pastor-Satorras, R. & Vespignani, A. Epidemic dynamics and endemic states in
294 complex networks. *Phys. Rev. E* **63**, 066117 (2001).
- 295 8. Gomes, M. G. M. & Montalbán, A. A SEIR model with variable susceptibility or
296 exposure to infection. *arXiv* (2020).
- 297 9. Gomes, M. G. M., et al. Individual variation in susceptibility or exposure to SARS-CoV-
298 2 lowers the herd immunity threshold. *medRxiv* 10.1101/2020.04.27.20081893 (2020).
- 299 10. Gomes, M. G. M., White, L. J. & Medley, G. F. Infection, reinfection, and vaccination
300 under suboptimal immune protection: Epidemiological perspectives. *J. Theor. Biol.* **228**,
301 539-549 (2004).

- 302 11. Gomes, M. G. M., Gjini, E., Lopes, J. S., Souto-Maior, C. & Rebelo, C. A theoretical
303 framework to identify invariant thresholds in infectious disease epidemiology. *J. Theor.*
304 *Biol.* **395**, 97-102 (2016).
- 305 12. Pollán, M., et al. Prevalence of SARS-CoV-2 in Spain (ENE-COVID): a nationwide,
306 population-based seroepidemiological study. *Lancet* 10.1016/s0140-6736(20)31483-5
307 (2020).
- 308 13. Sekine, T., et al. Robust T cell immunity in convalescent individuals with asymptomatic
309 or mild COVID-19. *medRxiv* 10.1101/2020.06.29.174888 (2020).
- 310 14. Gonçalves, G. Herd immunity: recent uses in vaccine assessment. *Expert Rev. Vaccines*
311 **7**, 1493-1506 (2008).
- 312 15. Fine, P., Eames, K. & Heymann, D. L. “Herd immunity”: a rough guide, *Clin. Infect.*
313 *Dis.* **52**, 911-916 (2011).
- 314 16. Ferrari, M. J., Bansal, S., Meyers, L. A. & Bjornstad, O. N. Network frailty and the
315 geometry of herd immunity. *Proc. R. Soc. B* **273**, 2743-2748 (2006).
- 316 17. Folegatti, P. M., et al. Safety and immunogenicity of the ChAdOx1 nCoV-19 vaccine
317 against SARS-CoV-2: a preliminary report of a phase 1/2, single-blind, randomised
318 controlled trial. *Lancet* 10.1016/S0140-6736(20)31604-4 (2020).
- 319 18. Zhu, F.-C., et al. Immunogenicity and safety of a recombinant adenovirus type-5-
320 vectored COVID-19 vaccine in healthy adults aged 18 years or older: a randomised,
321 double-blind, placebo-controlled, phase 2 trial. *Lancet* 10.1016/S0140-6736(20)31611-1
322 (2020).
- 323 19. Mossong, J., et al. Social contacts and mixing patterns relevant to the spread of
324 infectious diseases. *PLOS Med.* **5**, e74 (2008).
- 325 20. Prem, K., Cook, A. R. & Jit, M. Projecting social contact matrices in 152 countries using
326 contact surveys and demographic data. *PLOS Comput. Biol.* **13**, e1005697 (2017).
- 327 21. Zhang, J., et al. Changes in contact patterns shape the dynamics of the COVID-19
328 outbreak in China. *Science* **368**, 1481-1486 (2020).

- 329 22. Britton, T., Ball, F. & Trapman, P. A mathematical model reveals the influence of
330 population heterogeneity on herd immunity to SARS-CoV-2. *Science*
331 10.1126/science.abc6810 (2020).
- 332 23. Adam, D., et al. Clustering and superspreading potential of severe acute respiratory
333 syndrome coronavirus 2 (SARS-CoV-2) infections in Hong Kong. 10.21203/rs.3.rs-
334 29548/v1
- 335 24. Eubank, S., et al. Modelling disease outbreaks in realistic urban social networks. *Nature*
336 **429**, 180-184 (2004).
- 337 25. Grifoni, A., et al. Targets of T cell responses to SARS-CoV-2 coronavirus in humans
338 with COVID-19 disease and unexposed individuals. *Cell* **181**, 1489-1501.e15 (2020).
- 339 26. Le Bert, N., et al. SARS-CoV-2-specific T cell immunity in cases of COVID-19 and
340 SARS, and uninfected controls. *Nature* 10.1038/s41586-020-2550-z (2020).
- 341 27. Flaxman, S., et al. Estimating the effects of non-pharmaceutical interventions on
342 COVID-19 in Europe. *Nature* 10.1038/s41586-020-2405-7 (2020).
- 343

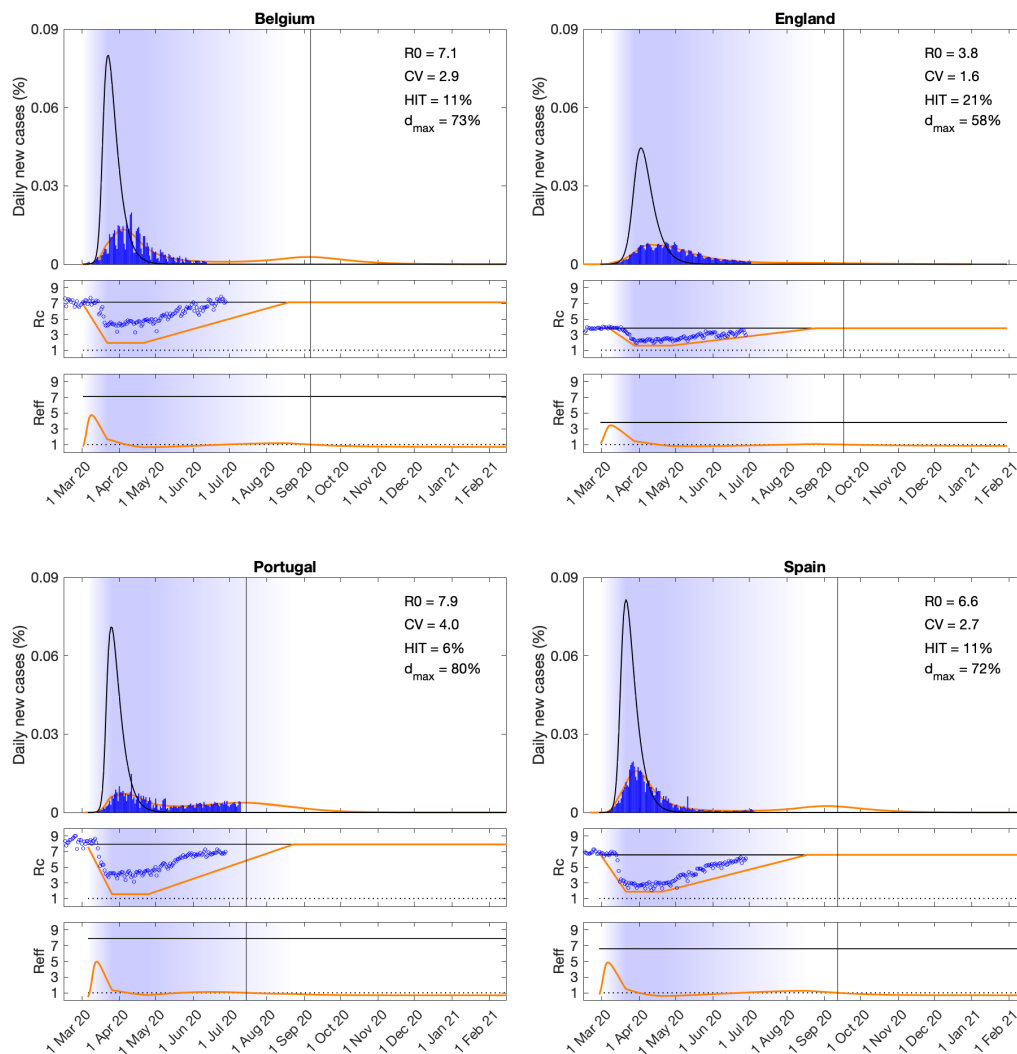
344



345

346 **Fig. 1| SARS-CoV-2 transmission with individual variation in susceptibility to**
 347 **infection.** Suppressed wave and subsequent dynamics in Belgium, England, Portugal
 348 and Spain (orange). Estimated epidemic in the absence of interventions revealing
 349 overshoot (black). Blue bars are daily new cases. Basic (R_0) and effective ($R_{eff} =$
 350 $\{\int \lambda(x)x[S(x) + \sigma R(x)] dx / \int \rho E(x) + I(x) dx\} \{\rho / \delta + 1 / \gamma\}$) reproduction
 351 numbers are displayed on shallow panels underneath the main plots. Blue shades
 352 represent social distancing (intensity reflected in R_0 trends and shade density).
 353 Susceptibility factors implemented as gamma distributions. Consensus parameter
 354 values (Methods): $\delta = 1/4$ per day; $\gamma = 1/4$ per day; and $\rho = 0.5$. Fraction of
 355 infected individuals identified as positive (reporting fraction): 0.06 (Belgium); 0.024
 356 (England); 0.09 (Portugal); 0.06 (Spain). Basic reproduction number, coefficients of
 357 variation and social distancing parameters estimated by Bayesian inference as
 358 described in Methods (estimates in Extended Data Table 1). Curves represent mean
 359 model predictions from 10^4 posterior samples. Orange shades represent 95% credible
 360 intervals. Vertical lines represent the expected time when herd immunity threshold
 361 will be achieved. Circles depict independent mobility data Google⁶ not used in our
 362 parameter estimation.
 363

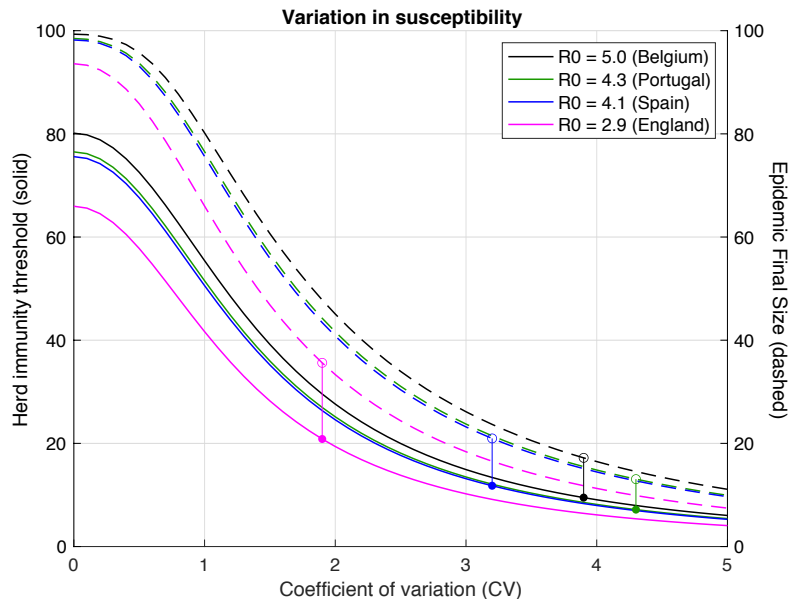
364



365

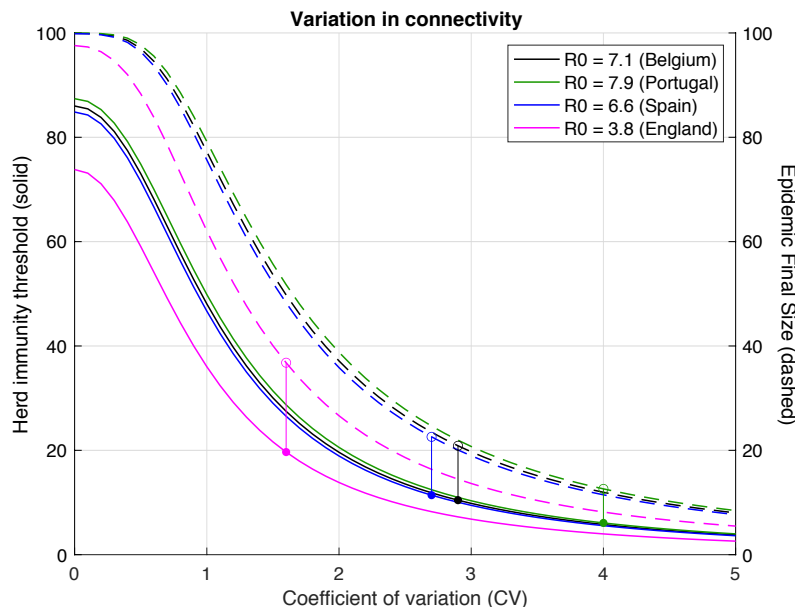
366 **Fig. 2| SARS-CoV-2 transmission with individual variation in exposure to**
 367 **infection.** Suppressed wave and subsequent dynamics in Belgium, England, Portugal
 368 and Spain (orange). Estimated epidemic in the absence of interventions revealing
 369 overshoot (black). Blue bars are daily new cases. Basic (R_0) and effective ($R_{eff} =$
 370 $\{\int \lambda(x)x[S(x) + \sigma R(x)] dx / \int \rho E(x) + I(x) dx\} \{\rho/\delta + 1/\gamma\}$) reproduction
 371 numbers are displayed on shallow panels underneath the main plots. Blue shades
 372 represent social distancing (intensity reflected in R_0 trends and shade density).
 373 Exposure factors implemented as gamma distributions. Consensus parameter values
 374 (Methods): $\delta = 1/4$ per day; $\gamma = 1/4$ per day; and $\rho = 0.5$. Fraction of infected
 375 individuals identified as positive (reporting fraction): 0.06 (Belgium); 0.024
 376 (England); 0.09 (Portugal); 0.06 (Spain). Basic reproduction number, coefficients of
 377 variation and social distancing parameters estimated by Bayesian inference as
 378 described in Methods (estimates in Extended Data Table 2). Curves represent mean
 379 model predictions from 10^4 posterior samples. Orange shades represent 95% credible
 380 intervals. Vertical lines represent the expected time when herd immunity threshold
 381 will be achieved. Circles depict independent mobility data Google⁶ not used in our
 382 parameter estimation.
 383

384



385

386



387

388 **Fig. 3| Herd immunity threshold with gamma-distributed susceptibility or**
 389 **exposure to infection.** Curves generated with the SEIR model (Equation 1-4)
 390 assuming values of R_0 estimated for the study countries (Extended Data Tables 1 and
 391 2) assuming gamma-distributed: susceptibility (top); connectivity (bottom). Herd
 392 immunity thresholds (solid curves) are calculated according to the formula $1 -$
 393 $(1/R_0)^{1/(1+CV^2)}$ for heterogeneous susceptibility and $1 - (1/R_0)^{1/(1+2CV^2)}$ for
 394 heterogeneous connectivity. Final sizes of the corresponding unmitigated epidemics
 395 are also shown (dashed).

396 **METHODS**

397 **Model structure and underlying assumptions**

398 The model presented here is a differential equation SEIR model, where susceptible
399 individuals become exposed at a rate that depends on their susceptibility, the number
400 of potentially infectious contacts they engage in, and the total number of infectious
401 people in the population per time unit. Upon exposure, individuals enter an
402 asymptomatic incubation phase, during which they slowly become infectious²⁹⁻³².
403 Thus, infectivity of exposed individuals is made to be 1/2 of that of infectious ones
404 ($\rho = 0.5$). After a few days, individuals develop symptoms – on average 4 days after
405 the exposure to the virus ($\delta = 1/4$) – and thus become fully infectious³³⁻³⁵. They
406 recover, i.e., they are no longer infectious 4 days after that ($\gamma = 1/4$), on average³⁶.

407 *Efficacy of acquired immunity*

408 We conducted the core of our analysis under the assumption that no reinfection occurs
409 after recovery due to acquired immunity ($\sigma = 0$). To analyse the sensitivity of these
410 results to leakage in immune response ($\sigma > 0$) we calculated herd immunity
411 thresholds (HIT) as a function of coefficients of variation (CV) for different values of
412 σ . The results displayed in Extended Data Figure 2 confirm the expectation that as the
413 efficacy of acquired immunity decreases (σ increases) larger percentages of the
414 population are infected before herd immunity is reached. Less intuitive is that there is
415 an upper bound for how much it is reasonable to increase σ before the system enters a
416 qualitatively different regime – the reinfection threshold¹⁰⁻¹¹ ($\sigma = 1/R_0$) – above
417 which infection becomes stably endemic and the notion of herd immunity threshold

418 no longer applies. Respiratory viruses are typically associated with epidemics
419 dynamics below the reinfection threshold.

420 *Effective reproduction number*

421 The effective reproduction number (R_{eff} , also denoted by R_e or R_t by other authors)
422 is a time-dependent quantity which we calculate as the incidence of new infections
423 divided by the total number of active infections (affected by ρ for individuals in E)
424 multiplied by the average duration of infection (also affected by ρ for individuals in
425 E)

$$426 \quad R_{eff}(t) = \frac{\int \lambda(x, t)x[S(x, t) + \sigma R(x, t)] dx}{\int \rho E(x, t) + I(x, t) dx} \left(\frac{\rho}{\delta} + \frac{1}{\gamma} \right). \quad (9)$$

427 *Assortative mixing*

428 In the main text we assumed random mixing among individuals, but human
429 connectivity patterns are assortative due societal structures and human behaviours. To
430 explore the sensitivity of our results to deviations from random mixing, we develop
431 an extended formalism that allows individuals to connect preferentially with those
432 with similar connectivity, formally $\lambda(x) =$
433 $(\beta/N)(\int y h(y - x)[\rho E(y) + I(y)] dy / \int yg(y) dy)$, where $h(y - x)$ is a normal
434 distribution on the difference between connectivity factors (Extended Data Figure 3).

435 *Dynamic coefficients of variation*

436 The formulation of the variable connectivity model in the main text assumes that
437 coefficients of variation are constant irrespective of interventions. Social distancing
438 has been assumed to reduce connectivity of every individual by the same factor (from

439 x to $[1 - d]x$) leaving the coefficient of variation unchanged. The possibility that CV
440 might reduce with social distancing (d), causing a drop in the intensity of selection,
441 might affect our results. To study sensitivity to this type of CV dynamics, we
442 formulate an extended model where connectivity is reformulated as $(1 - d)[1 +$
443 $(1 - d)(x - 1)]$, and whose CV decreases with social distancing (Extended Data
444 Figure 4). This does not change the way the model is written but special care is
445 needed in analysis and interpretation to account for the new dynamics. The basic
446 reproduction number, in particular, depends explicitly on a CV which is now
447 dependent on social distancing

$$448 \quad R_0 = [1 + CV(d)^2]\beta \left(\frac{\rho}{\delta} + \frac{1}{\gamma} \right), \quad (10)$$

449 which is noticeable in the curvilinear shape of the controlled R_0 (R_c) trajectories
450 (Extended Data Figure 5).

451 *Non-pharmaceutical interventions*

452 We implemented non-pharmaceutical interventions (NPI) as a gradual decrease in
453 viral transmissibility in the population and thus a lowering of the controlled and
454 effective reproduction numbers (R_c and R_{eff}). Once containment measures are put in
455 place in each country, we postulate it takes 21 days until the maximum effectiveness
456 of social distancing measures is reached. In the simulations presented throughout we
457 have held this condition (maximum “lockdown” efficacy) for 30 days, after which
458 period, social distancing measures are progressively relaxed, slowly returning to pre-
459 pandemic conditions. Both the implementation and relaxing of the social distancing
460 measures are imposed to be linear in this scheme.

461 **Bayesian Inference**

462 The model laid out above is amenable to theoretical exploration as presented in the
463 main manuscript and provides a perfect framework for inference. Fundamentally, to
464 be able to reproduce the inception of any epidemic, we would need to estimate when
465 local transmission started to occur (t_0), and the pace at which individuals infected
466 each other in the very early stages of the epidemic (R_0). All countries, to different
467 extents and at different timepoints of the epidemic, enforced some combination of
468 social distancing measures. To fully understand the interplay between herd immunity
469 and the impact of NPIs, we then set out to estimate the time at which social distancing
470 measures started to have an impact on daily incidence (t_0^d), what their maximum
471 effectiveness (d_{max}) is, the basic reproduction number (R_0) and what the underlying
472 variance in heterogeneity is for both susceptibility to infection and number of
473 infectious contacts.

474 In order to preserve identifiability, we made two simplifying assumptions: (i) the
475 fraction of infectious individuals reported as COVID-19 cases (reporting fraction) is
476 constant throughout the study period and is comparable between countries
477 proportionally to the number of tests performed per person; (ii) local transmission
478 starts (t_0) when countries/regions report 1 case per 5 million population in one day.
479 To calculate the reporting rates, we used the Spanish national serological survey¹² as a
480 reference and divided the total number of reported cases up to May 11th by the
481 estimated number of people that had been exposed to the virus. This gives us a
482 reporting rate for Spain around 6%. Unfortunately, there are no other national
483 serological surveys that could inform the proportion of the population infected in
484 other countries, so we had to extrapolate the reporting rate for those. Assuming the

485 reporting rate is highly dependent on the testing effort employed in each country,
486 reflected in the number of tests per individual, we estimate the reporting rate by
487 scaling the reporting rate recorded in Spain according to the ratio of PCR tests per
488 person in other countries relative to the Spanish reference of 0.9 tests per thousand
489 people (<https://ourworldindata.org/coronavirus-testing>). This produced estimated case
490 reporting rates (ratio of reported cases to infections) of 9% for Portugal, 6% for
491 Belgium (and Spain) and 2.4% for England.

492 Whist national case and mortality data is easily available for most countries, more
493 spatially resolute data is difficult to find in the public domain. Thus, we restricted our
494 analysis to countries for which disaggregated regional case data was easily available.
495 We collected the data at two time points. First, we compiled all available data from
496 the day the countries started reporting COVID-19 cases to the initial collection date
497 (May 20th) and later collated available data from May 21st to July 10th.

498 Parameter estimation was performed with the software MATLAB, using PESTO
499 (Parameter ESTimation Toolbox)³⁷, and assuming the reported case data can be
500 accurately described by a Poisson process. We first fixed the beginning of local
501 transmission (parameter t_0) in each data series as the day in which reported cases
502 surpassed 1 in 5 million individuals. Next, we optimized the model for the set of
503 parameters $\theta = \{R_0, CV, t_0^d, d_{max}\}$ by maximizing the logarithm of the likelihood
504 (LL) (Equation 11) of observing the daily reported number of cases in each country
505 $D = \{(k, \tilde{y}_k)\}_{k=0}^n$:

$$LL(\theta|D) = -\sum_{k=1}^n y(k, \theta) + \left(\sum_{k=1}^n \tilde{y}(k) \ln(y(k, \theta)) \right) - \ln \left(\prod_{k=1}^n \tilde{y}(k)! \right) \quad (11)$$

506 in which $y(k, \theta)$ is the simulated model output number of COVID-19 cases at day k
507 (with respect to t_0), and n is the total number of days included in the analysis for each
508 country.

509 When fitting the model to disaggregated data, we follow the procedure outlined above
510 and estimate region-specific R_0 and CV , with common t_0^d and d_{max} . To ensure that
511 the estimated maximum is a global maximum, we performed 50 multi-starts
512 optimizations, and selected the combination of parameters resulting in the maximal
513 Loglikelihood as a starting point for 10^4 Markov Chain Monte-Carlo iterations. From
514 the resulting posterior distributions, we extract the median estimates for each
515 parameter and the respective 95% credible intervals for the set of parameters $\theta =$
516 $\{R_0, CV, t_0^d, d_{max}\}$. We used uniformly distributed priors with ranges $\{1-9, 0.0025-$
517 $8, 1-60, 0-0.7\}$.

518 This fitting procedure was applied to 4 countries (Belgium, England, Portugal and
519 Spain) for both the national and disaggregated case data series and repeated for each
520 of the 4 model variants considered here (homogeneous, heterogeneous susceptibility,
521 heterogeneous connectivity with constant CV , and heterogeneous connectivity with
522 CV reducing in proportion to social distancing). In the fitting procedures using sub-
523 national data, we assumed regions had the same start date for interventions that
524 mitigate transmission (t_0^d), and that these measures produced the same maximum
525 impact on transmission (d_{max}) everywhere. Thus, the only region-specific parameters
526 to be estimated are $\{R_{0i}, CV_i\}$. Parameter estimates obtained from each of the model
527 variants are displayed in Extended Data Table 1 (heterogeneity in susceptibility),
528 Extended Data Table 2 (heterogeneity in connectivity with constant CV), Extended
529 Data Table 3 (heterogeneity in connectivity with dynamic CV) and Extended Data

530 Table 4 (homogeneous model), are comparable to those obtained in other studies^{27,38-}
531 ⁴³. Finally, we apply the Akaike information criterion (AIC) for each estimation
532 procedure to inform on the quality of each model's fit to the datasets of reported cases
533 (Extended Data Table 5). In all cases, heterogeneous models are preferred over the
534 homogeneous approximation. Homogeneous models systematically fail to fit the
535 maintenance of low numbers of cases after the relaxation of social distancing
536 measures in many countries and regions (images not shown). The three heterogeneous
537 models are roughly equally well supported by the data used in this study. Further
538 research should complement this with discriminatory data types and hybrid models to
539 enable the integration of different forms of individual variation.

540 **Data and code availability**

541 Datasets are publicly available at the respective national ministry of health websites
542 (44-48). Core models implemented in MATLAB available from:
543 <https://github.com/mgmgomes1/covid>

544

- 545 28. Wei, W. E., et al. Presymptomatic Transmission of SARS-CoV-2 — Singapore, January
546 23–March 16, 2020. *MMWR Morb Mortal Wkly Rep* [Internet]. 2020 Apr 10 [cited
547 2020 May 4];69(14):411–5. Available from:
548 http://www.cdc.gov/mmwr/volumes/69/wr/mm6914e1.htm?s_cid=mm6914e1_w
- 549 29. To, K. K. W., et al. Temporal profiles of viral load in posterior oropharyngeal saliva
550 samples and serum antibody responses during infection by SARS-CoV-2: an
551 observational cohort study. *Lancet Infect. Dis.* **20**, 565-74 (2020).
- 552 30. Arons, M. M., et al. Presymptomatic SARS-CoV-2 Infections and Transmission in a
553 Skilled Nursing Facility. *N. Engl. J. Med.* **382**, 2081-2090 (2020).

- 554 31. He, X., et al. Temporal dynamics in viral shedding and transmissibility of COVID-19.
555 *Nat. Med.* **26**, 672-675 (2020).
- 556 32. Lauer, S. A., et al. The Incubation Period of Coronavirus Disease 2019 (COVID-19)
557 From Publicly Reported Confirmed Cases: Estimation and Application. *Ann. Intern.*
558 *Med.* **172**, 577-582 (2020).
- 559 33. Li, Q., et al. Early transmission dynamics in Wuhan, China, of novel coronavirus-
560 infected pneumonia. *N. Engl. J. Med.* **382**, 1199-1207 (2020).
- 561 34. Zhang, J., et al. Evolving epidemiology and transmission dynamics of coronavirus
562 disease 2019 outside Hubei province, China: A descriptive and modelling study. *Lancet*
563 *Infect. Dis.* **20**, 793-802 (2020).
- 564 35. Nishiura, H., Linton, N. M. & Akhmetzhanov, A. R. Serial interval of novel coronavirus
565 (COVID-19) infections. *Int. J. Infect. Dis.* **93**, 284-6 (2020).
- 566 36. Stapor, P., et al. PESTO: Parameter ESTimation TOolbox. *Bioinformatics* **34**, 705-707
567 (2018).
- 568 37. Jarvis, C. I., et al. Quantifying the impact of physical distance measures on the
569 transmission of COVID-19 in the UK. *BMC Medicine* **18**, 124 (2020).
- 570 38. Prem, K., et al. The effect of control strategies to reduce social mixing on outcomes of
571 COVID-19 epidemic in Wuhan, China: a modelling study. *Lancet Public Health* **5**, e261-
572 e270.
- 573 39. Tian, H., et al. An investigation of transmission control measures during the first 50 days
574 of the COVID-19 epidemic in China. *Science* **368**, 638-642.
- 575 40. Kucharski, A. J., et al. Effectiveness of isolation, testing, contact tracing and physical
576 distancing on reducing transmission of SARS-CoV-2 in different settings: a
577 mathematical modelling study. *Lancet Infect. Dis.* 10.1016/s1473-3099(20)30457-6
578 (2020).
- 579 41. Salje, H., et al. Estimating the burden of SARS-CoV-2 in France. *Science* **369**, 208-211
580 (2020).

- 581 42. Di Domenico, L., Pullano, G., Sabbatini, C. E., Boelle, P.-Y. & Colizza, V. Expected
582 impact of lockdown in Île-de-France and possible exit strategies. *medRxiv*
583 10.1101/2020.04.13.20063933 (2020).
- 584 43. [https://ourworldindata.org/coronavirus-testing#source-information-country-by-](https://ourworldindata.org/coronavirus-testing#source-information-country-by-country)
585 [country](https://ourworldindata.org/coronavirus-testing#source-information-country-by-country). Accessed on July 10th 2020.
- 586 44. <https://cnecovid.isciii.es/covid19>.
- 587 45. <https://covid-19.sciensano.be/nl/covid-19-epidemiologische-situatie>.
- 588 46. <https://covid19.min-saude.pt/ponto-de-situacao-atual-em-portugal>.
- 589 47. <https://coronavirus.data.gov.uk>.

590

591 **Acknowledgements**

592 We thank Jan Hasenauer and Antonio Montalbán for helpful discussions concerning
593 statistical inference and mathematics, respectively. R.M.C. and M.U.F. receive
594 scholarships from the Conselho Nacional de Desenvolvimento Científico e
595 Tecnológico (CNPq), Brazil.

596

597 **Author contributions**

598 M.G.M.G. conceived the study. R.A. and R.M.C. and M.G.M.G. performed the
599 analyses. All authors interpreted the data and wrote the paper.

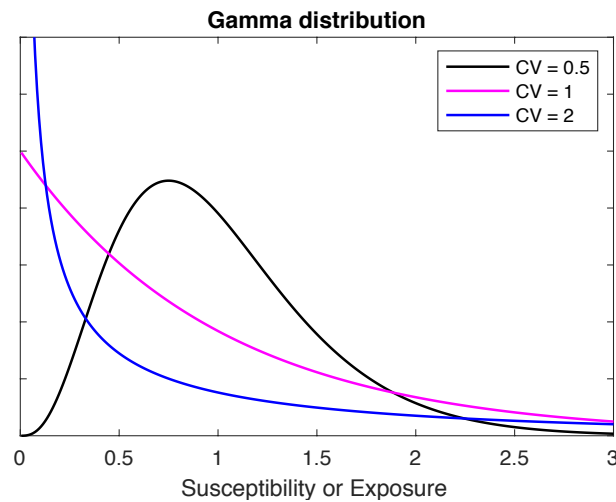
600

601 **Competing interests**

602 The authors declare no competing interests.

603

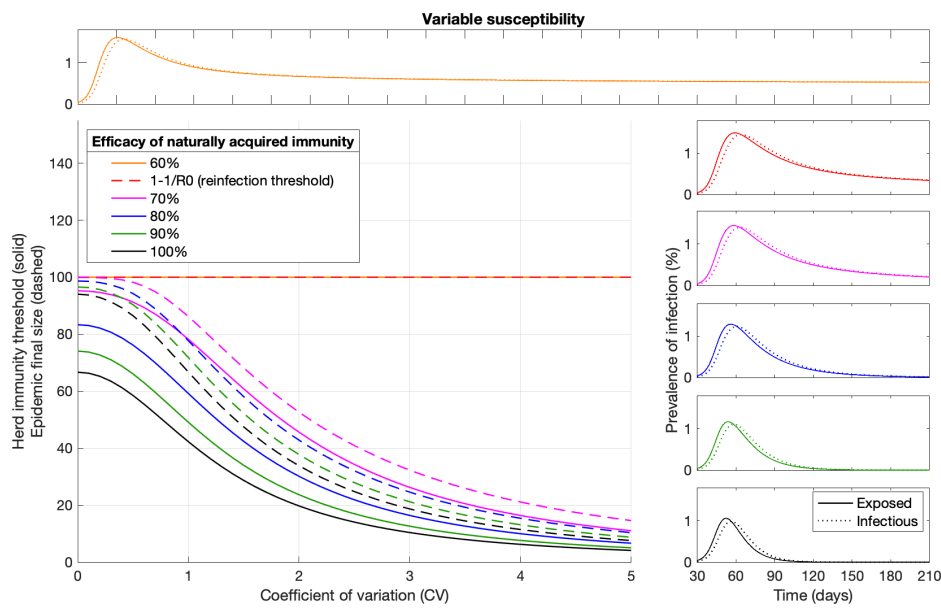
604



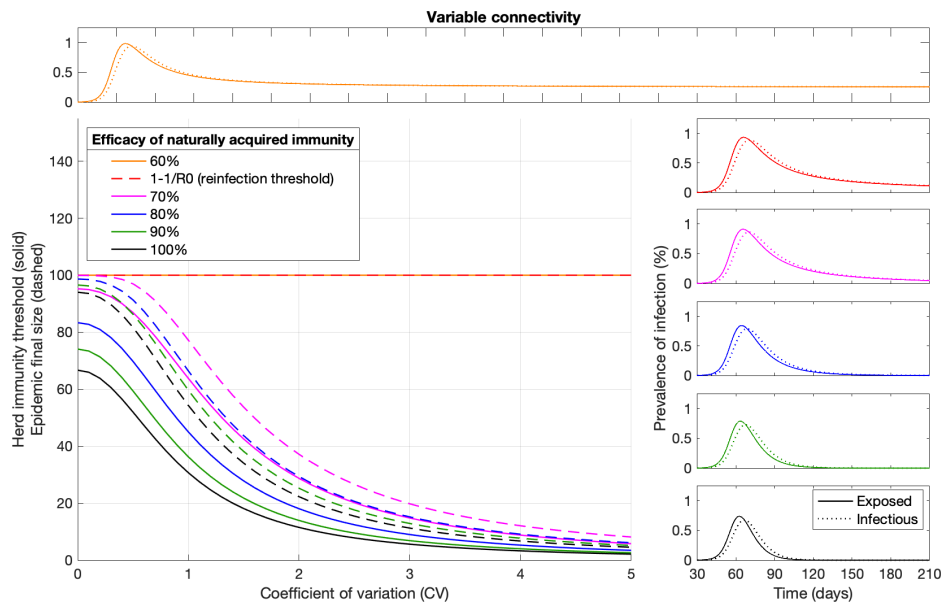
605

606 **Extended Data Fig. 1 | Distributions used for variable susceptibility and**
607 **connectivity.** Gamma distribution probability density functions with mean 1 and
608 various coefficients of variation: $[x^{1/CV^2-1}e^{-x/CV^2}]/[\Gamma(1/CV^2)CV^{(2/CV^2)}]$, where Γ
609 is the Gamma function. For numerical implementations we discretized gamma
610 distributions into N bins, calculated the susceptibility or connectivity factor as well as
611 the fraction of the population in each bin, and derived the associated $4N$ -dimensional
612 systems of ordinary differential equations.
613

614



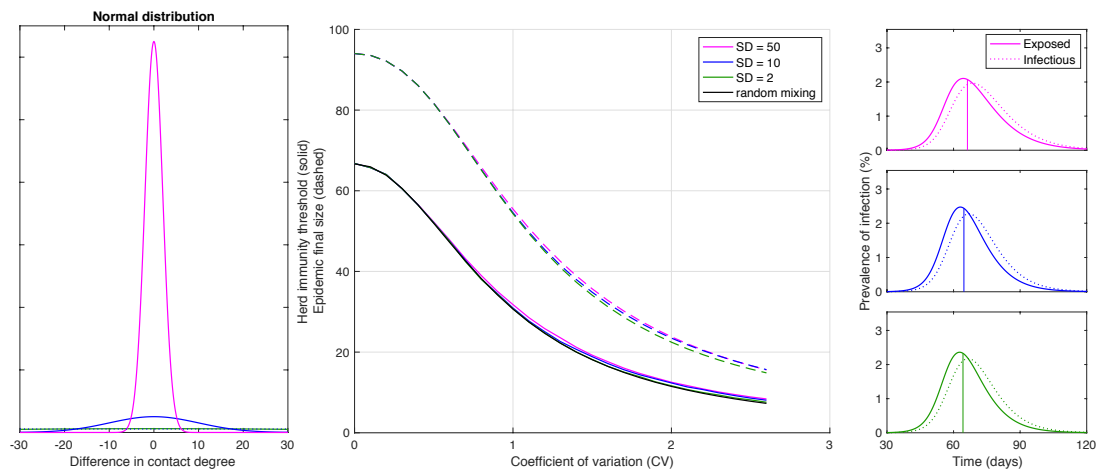
615



616

617 **Extended Data Fig. 2| Herd immunity threshold and epidemic final size with**
 618 **reinfection.** Curves in the main panels generated with the SEIR model (Equation 1-4)
 619 assuming $R_0 = 3$ and gamma-distributed susceptibility (top) or connectivity (bottom).
 620 Efficacy of acquired immunity is captured by a reinfection parameter σ , potentially
 621 ranging between $\sigma = 0$ (100% efficacy) and $\sigma = 1$ (0 efficacy). This illustration
 622 depicts final sizes of unmitigated epidemics and associated HIT curves for 6 values of
 623 σ : $\sigma = 0$ (black); $\sigma = 0.1$ (green); $\sigma = 0.2$ (blue); $\sigma = 0.3$ (magenta); $\sigma = 1/3$ (red);
 624 and $\sigma = 0.4$ (orange);. Above $\sigma = 1/R_0$ (reinfection threshold (Gomes et al 2004;
 625 2016)) the infection becomes stably endemic and there is no herd immunity threshold.
 626 Representative epidemics of the regime $\sigma \leq 1/R_0$ are shown on the right while the
 627 regime $\sigma > 1/R_0$ is illustrated on top. All depicted dynamics are based on the
 628 rightmost CVs represented on the main panel.
 629

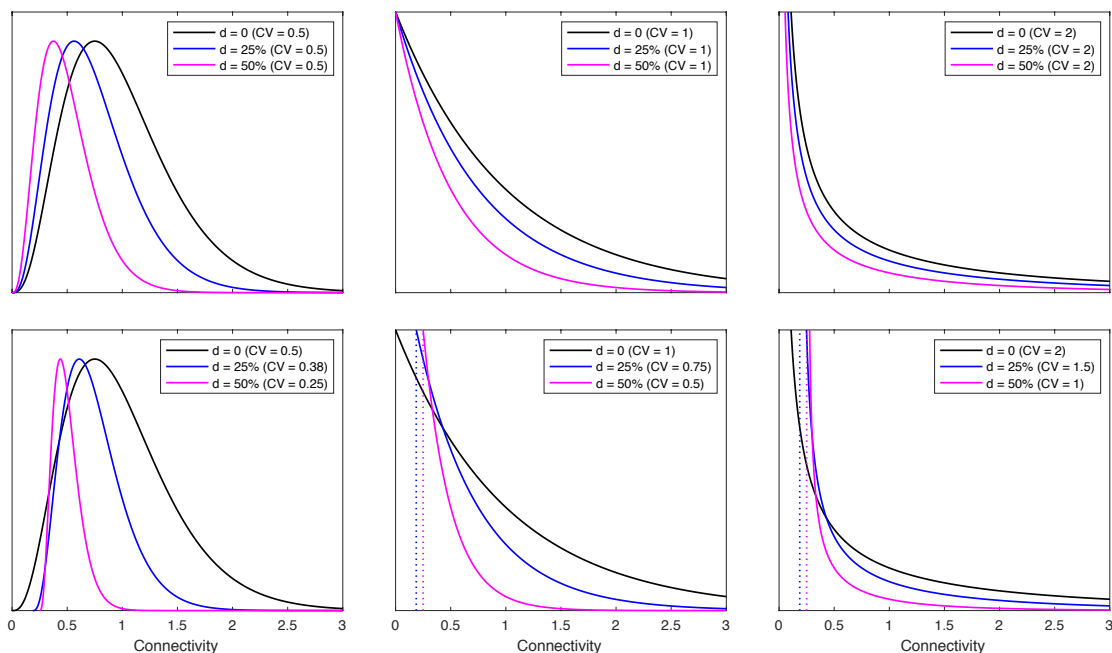
630



631

632 **Extended Data Fig. 3| Herd immunity threshold and epidemic final size with**
 633 **gamma-distributed exposure to infection and assortative mixing.** Curves in
 634 central panel generated with the SEIR model (Equation 1-4) assuming $R_0 = 3$ and
 635 gamma-distributed connectivity. Assortative mixing is implemented by imposing a
 636 normal distribution for contact preferences such that individuals contact preferentially
 637 with those with the similar contact degree (left). This illustration used normal
 638 distributions with standard deviation $SD = 50$ (green); $SD = 10$ (blue); and $SD = 2$
 639 (magenta). More assortative mixing leads to more skewed epidemics. Herd immunity
 640 thresholds were calculated numerically as the percentage of the population no longer
 641 susceptible when new outbreaks are effectively prevented (approximately when the
 642 exposed fraction crosses the peak in the absence of mitigation). Final sizes of the
 643 corresponding unmitigated epidemics are also shown. Representative epidemics are
 644 depicted on the right based on the rightmost CVs represented on the main panel (with
 645 vertical lines marking the point when herd immunity is achieved).
 646

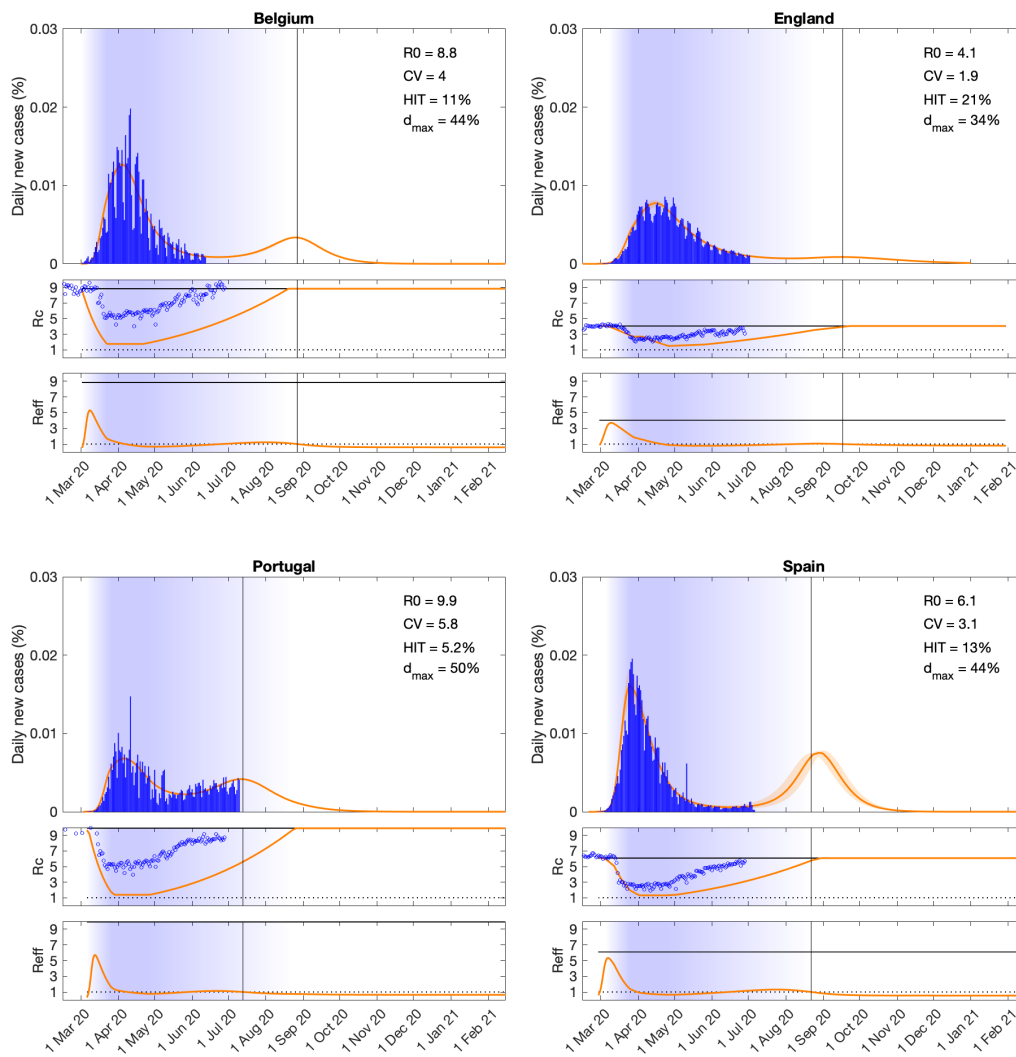
647



648

649 **Extended Data Fig. 4| Connectivity distributions with reducing coefficient of**
 650 **variation in proportion to social distancing.** Individual variation in connectivity is
 651 originally implemented as a gamma distribution of mean 1 parameterised by the
 652 coefficient of variation (CV) (black). Social distancing is initially implemented as a
 653 reduction in connectivity by the same factor to every individual, from x to $(1 - d)x$
 654 (top panels). Sensitivity of the results to the possibility that CV might reduce with
 655 social distancing with replicated the analyses with a model connectivity is
 656 reformulated as $(1 - d)[1 + (1 - d)(x - 1)]$ (bottom panels).
 657

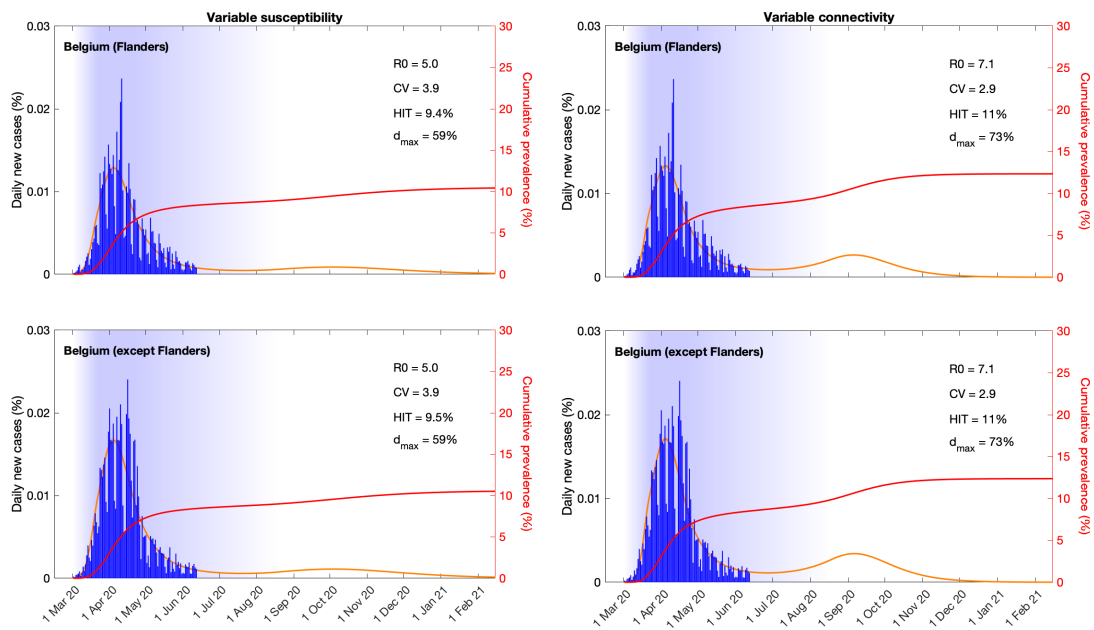
658



659

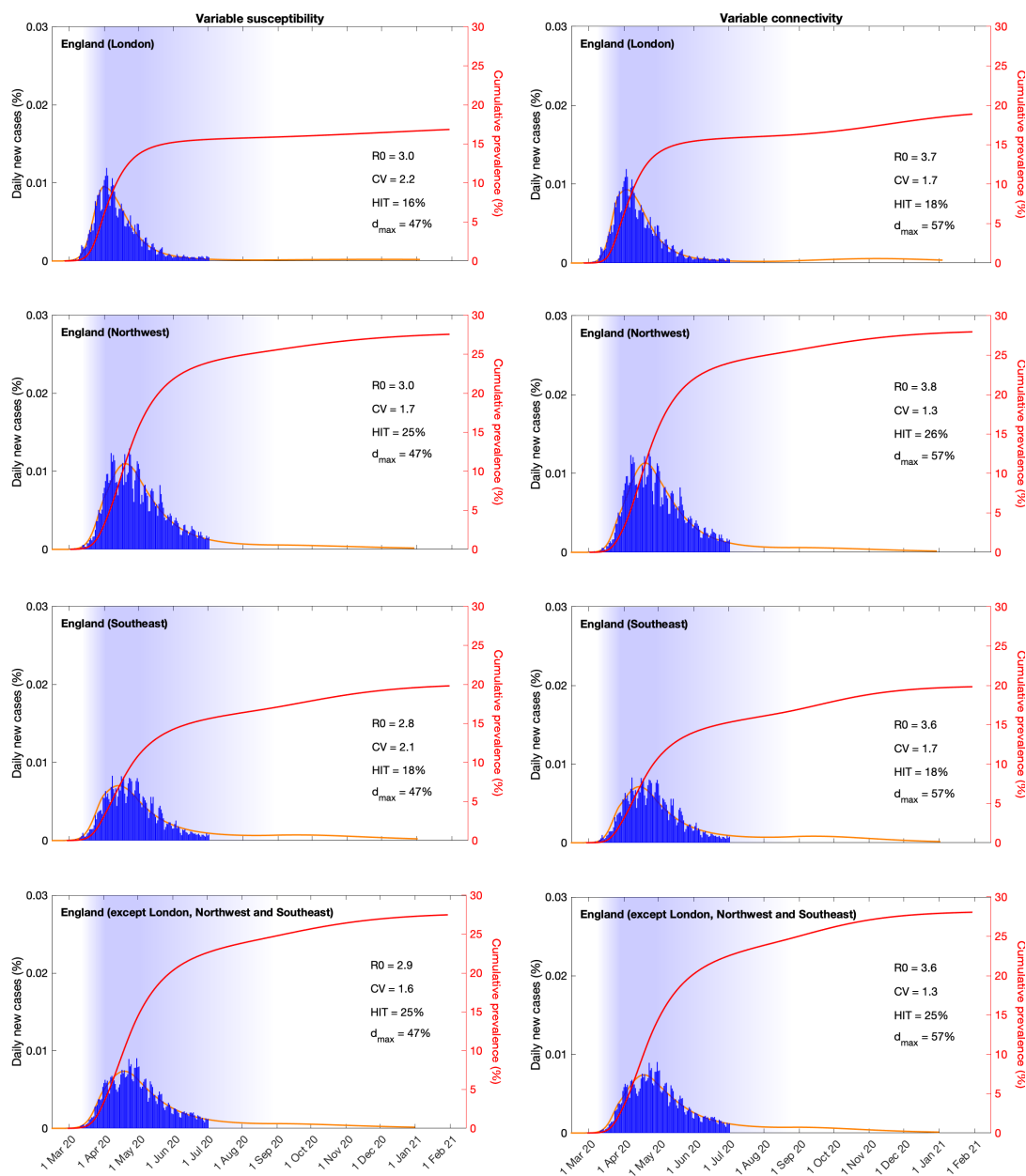
660 **Extended Data Fig. 5| SARS-CoV-2 transmission with individual variation in**
 661 **exposure reduced by social distancing.** Suppressed wave and subsequent dynamics
 662 in Belgium, England, Portugal and Spain. Blue bars are daily new cases. Basic (R_0)
 663 and effective ($R_{eff} = \{\int \lambda(x)x[S(x) + \sigma R(x)] dx / \int \rho E(x) + I(x) dx\} \{\rho / \delta +$
 664 $1/\gamma\}$) reproduction numbers are displayed on shallow panels underneath the main
 665 plots. Blue shades represent social distancing (intensity reflected in R_0 trends and
 666 shade density). Exposure factors implemented as gamma distributions. Consensus
 667 parameter values (Methods): $\delta = 1/4$ per day; $\gamma = 1/4$ per day; and $\rho = 0.5$.
 668 Fraction of infected individuals identified as positive (reporting fraction): 0.06
 669 (Belgium); 0.024 (England); 0.09 (Portugal); 0.06 (Spain). Basic reproduction
 670 number, coefficients of variation and social distancing parameters estimated by
 671 Bayesian inference as described in Methods (estimates in Extended Data Table 3).
 672 Curves represent mean model predictions from 10^4 posterior samples. Orange shades
 673 represent 95% credible intervals. Vertical lines represent the expected time when herd
 674 immunity threshold will be achieved. Circles depict independent mobility data
 675 (Google 2020) not used in our parameter estimation.
 676

677



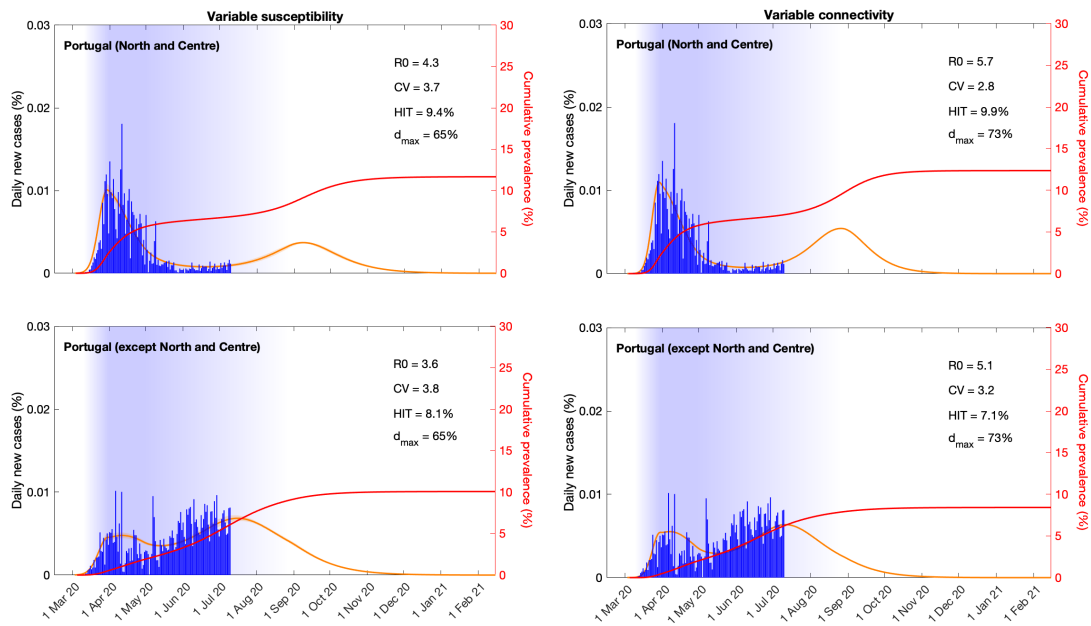
678 **Extended Data Fig. 6 | SARS-CoV-2 transmission at subnational levels in Belgium.**
 679 Suppressed wave and subsequent dynamics in Flanders and the rest of Belgium, with
 680 individual variation in susceptibility (left) or exposure (right). Blue bars are daily new
 681 cases. Shades represent social distancing (intensity reflected in shade density).
 682 Susceptibility or exposure factors implemented as gamma distributions. Consensus
 683 parameter values (Methods): $\delta = 1/4$ per day; $\gamma = 1/4$ per day; and $\rho = 0.5$.
 684 Fraction of infected individuals identified as positive (reporting fraction): 0.06. Basic
 685 reproduction number, coefficients of variation and social distancing parameters
 686 estimated by Bayesian inference as described in Methods (estimates in Extended Data
 687 Table 1 and 2). Curves represent mean model predictions from 10^4 posterior samples.
 688 Orange shades represent 95% credible intervals. Red curves represent cumulative
 689 infected percentages.
 690

691



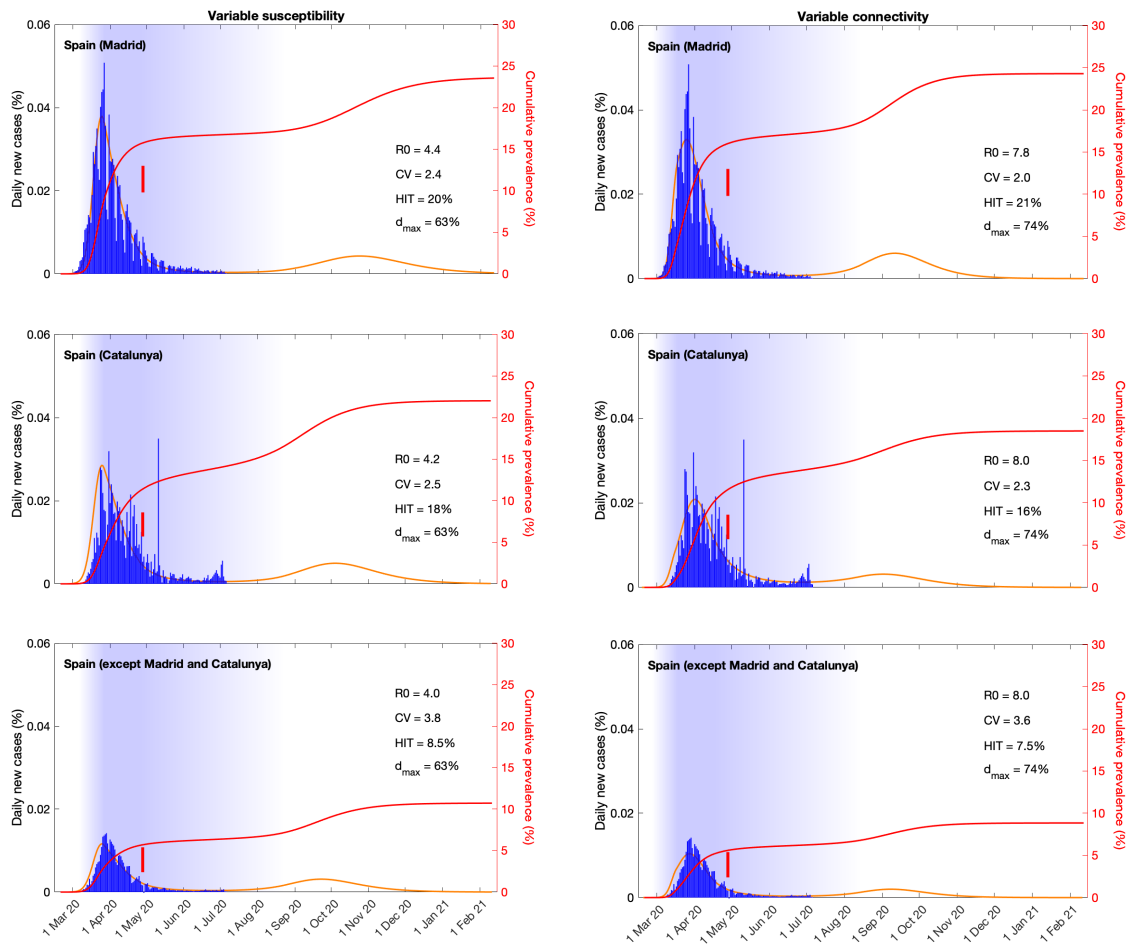
692 **Extended Data Fig. 7 | SARS-CoV-2 transmission at subnational levels in England.**
 693 Suppressed wave and subsequent dynamics in London, Northwest, Southeast and the
 694 rest of England, with individual variation in susceptibility (left) or exposure (right).
 695 Blue bars are daily new cases. Shades represent social distancing (intensity reflected
 696 in shade density). Susceptibility or exposure factors implemented as gamma
 697 distributions. Consensus parameter values (Methods): $\delta = 1/4$ per day; $\gamma = 1/4$ per
 698 day; and $\rho = 0.5$. Fraction of infected individuals identified as positive (reporting
 699 fraction): 0.024. Basic reproduction number, coefficients of variation and social
 700 distancing parameters estimated by Bayesian inference as described in
 701 Methods (estimates in Extended Data Table 1 and 2). Curves represent mean model
 702 predictions from 10^4 posterior samples. Orange shades represent 95% credible
 703 intervals. Red curves represent cumulative infected percentages.
 704

705



706 **Extended Data Fig. 8| SARS-CoV-2 transmission at subnational levels in Portugal.**
 707 Suppressed wave and subsequent dynamics in the North and Centre regions versus the
 708 rest of Portugal, with individual variation in susceptibility (left) or exposure (right).
 709 Blue bars are daily new cases. Shades represent social distancing (intensity reflected
 710 in shade density). Susceptibility or exposure factors implemented as gamma
 711 distributions. Consensus parameter values (Methods): $\delta = 1/4$ per day; $\gamma = 1/4$ per
 712 day; and $\rho = 0.5$. Fraction of infected individuals identified as positive (reporting
 713 fraction): 0.09. Basic reproduction number, coefficients of variation and social
 714 distancing parameters estimated by Bayesian inference as described in Methods
 715 (estimates in Extended Data Table 1 and 2). Curves represent mean model predictions
 716 from 10^4 posterior samples. Orange shades represent 95% credible intervals. Red
 717 curves represent cumulative infected percentages.
 718

719



720 **Extended Data Fig. 9 | SARS-CoV-2 transmission at subnational levels in Spain.**
 721 Suppressed wave and subsequent dynamics in Madrid, Catalunya and the rest of
 722 Spain, with individual variation in susceptibility (left) or exposure (right). Blue bars
 723 are daily new cases. Shades represent social distancing (intensity reflected in shade
 724 density). Susceptibility or exposure factors implemented as gamma distributions.
 725 Consensus parameter values (Methods): $\delta = 1/4$ per day; $\gamma = 1/4$ per day; and $\rho =$
 726 0.5 . Fraction of infected individuals identified as positive (reporting fraction): 0.06 .
 727 Basic reproduction number, coefficients of variation and social distancing parameters
 728 estimated by Bayesian inference as described in Methods (estimates in Extended Data
 729 Table 1 and 2). Curves represent mean model predictions from 10^4 posterior samples.
 730 Orange shades represent 95% credible intervals. Red curves represent cumulative
 731 infected percentages and vertical red segments mark seroprevalences (95% CI)
 732 according to a recent study¹².
 733

734 **Extended Data Table 1| Estimated parameters for heterogeneous susceptibility**
 735 **model.** Estimates generated from model fit to the national datasets are in the grey
 736 shaded rows. The remaining rows provide the region-specific estimates. Best
 737 parameter estimates are presented as a bold median bounded by the lower and upper
 738 ends for the 95% credible interval. Model runs are initiated on the day (t_0) when
 739 reported cases surpassed 1 in 5 million individuals: Belgium (day 1); England (day
 740 29); Portugal (day 3); Spain (day 8).
 741

Country/Region	R_0			CV			$1 - d_{max}$			t_0^d		
Belgium	4.99	5.03	5.06	3.87	3.88	3.91	0.40	0.40	0.41	1.00	1.01	1.12
Flanders	4.96	5.00	5.02	3.89	3.91	3.93	0.41	0.41	0.41	1.00	1.02	1.15
Rest	4.97	5.01	5.03	3.87	3.89	3.91						
Portugal	4.23	4.26	4.31	4.22	4.26	4.30	0.30	0.31	0.31	7.37	7.71	7.91
North/Centre	3.54	3.58	3.61	3.72	3.76	3.79	0.34	0.35	0.35	7.51	7.73	8.00
Rest	4.27	4.32	4.36	3.69	3.72	3.74						
Spain	4.08	4.10	4.11	3.20	3.21	3.22	0.37	0.37	0.37	16.02	16.13	16.23
Madrid	4.38	4.39	4.39	2.37	2.37	2.38	0.37	0.37	0.37	16.40	16.41	16.44
Catalunya	4.20	4.21	4.21	2.49	2.50	2.50						
Rest	3.96	3.97	3.97	3.80	3.81	3.82						
England	2.93	2.94	2.95	1.94	1.94	1.95	0.52	0.52	0.52	40.56	40.69	40.80
London	2.95	2.96	2.96	2.24	2.24	2.24	0.52	0.53	0.53	41.35	41.51	41.64
NorthWest	3.03	3.04	3.05	1.66	1.67	1.68						
SouthEast	2.80	2.81	2.82	2.07	2.07	2.07						
Rest	2.88	2.88	2.89	1.64	1.64	1.65						

742
 743
 744

745 **Extended Data Table 2| Estimated parameters for heterogeneous connectivity**
 746 **model (constant CV).** Estimates generated from model fit to the national datasets are
 747 in the grey shaded rows. The remaining rows provide the region-specific estimates.
 748 Best parameter estimates are presented as a bold median bounded by the lower and
 749 upper ends for the 95% credible interval. Model runs are initiated on the day (t_0)
 750 when reported cases surpassed 1 in 5 million individuals: Belgium (day 1); England
 751 (day 29); Portugal (day 3); Spain (day 8).
 752

Country/Region	R_0			CV			$1 - d_{max}$			t_0^d		
Belgium	7.12	7.14	7.17	2.86	2.87	2.88	0.27	0.27	0.27	1.00	1.01	1.04
Flanders	7.09	7.11	7.13	2.86	2.87	2.89	0.27	0.27	0.28	1.00	1.01	1.03
Rest	7.11	7.13	7.15	2.86	2.87	2.89						
Portugal	7.76	7.94	8.14	4.01	4.04	4.09	0.19	0.20	0.20	2.67	2.98	3.27
North/Centre	5.06	5.08	5.09	3.24	3.24	3.24	0.25	0.25	0.25	7.21	7.22	7.24
Rest	5.68	5.69	5.69	2.79	2.81	2.83						
Spain	6.59	6.60	6.60	2.73	2.73	2.73	0.28	0.28	0.28	10.00	10.01	10.02
Madrid	7.81	7.83	8.82	1.98	1.99	2.06	0.24	0.26	0.26	5.38	7.02	7.06
Catalunya	8.00	8.02	9.00	2.33	2.34	2.43						
Rest	7.97	7.99	8.96	3.58	3.59	3.72						
England	3.81	3.82	3.83	1.55	1.55	1.55	0.42	0.42	0.42	36.45	36.52	36.61
London	3.70	3.70	3.71	1.69	1.69	1.70	0.43	0.43	0.43	37.50	37.52	37.55
NorthWest	3.83	3.83	3.84	1.32	1.32	1.32						
SouthEast	3.58	3.59	3.59	1.66	1.67	1.68						
Rest	3.60	3.60	3.61	1.30	1.31	1.31						

753
 754
 755
 756

757 **Extended Data Table 3| Estimated parameters for heterogeneous connectivity**
 758 **model (dynamic CV).** Estimates generated from model fit to the national datasets are
 759 in the grey shaded rows. The remaining rows provide the region-specific estimates.
 760 Best parameter estimates are presented as a bold median bounded by the lower and
 761 upper ends for the 95% credible interval. Model runs are initiated on the day (t_0)
 762 when reported cases surpassed 1 in 5 million individuals: Belgium (day 1); England
 763 (day 29); Portugal (day 3); Spain (day 8).
 764

Country/Region	R_0			CV			$1 - d_{max}$			t_0^d		
Belgium	8.79	8.84	8.88	3.98	4.00	4.02	0.56	0.56	0.56	1.00	1.01	1.05
Flanders	8.78	8.82	8.86	3.98	4.00	4.02	0.56	0.56	0.56	1.00	1.01	1.04
Rest	8.82	8.86	8.89	3.98	4.00	4.02						
Portugal	9.86	9.92	9.95	5.73	5.77	5.80	0.50	0.50	0.50	3.00	3.01	3.07
North/Centre	6.65	6.72	6.80	3.75	3.78	3.81	0.56	0.57	0.57	5.84	6.02	6.19
Rest	5.98	6.05	6.13	4.09	4.14	4.19						
Spain	5.97	6.09	6.10	3.04	3.09	3.10	0.56	0.56	0.56	14.46	14.50	14.89
Madrid	6.19	6.20	6.21	2.43	2.43	2.44	0.57	0.57	0.57	13.80	13.81	13.83
Catalunya	6.30	6.32	6.33	2.61	2.62	2.62						
Rest	6.34	6.35	6.36	3.80	3.81	3.82						
England	4.01	4.05	4.09	1.90	1.92	1.93	0.66	0.66	0.66	36.79	37.03	37.29
London	3.78	3.79	3.80	1.99	2.00	2.01	0.67	0.67	0.67	39.06	39.20	39.28
NorthWest	3.91	3.92	3.94	1.64	1.65	1.66						
SouthEast	3.67	3.69	3.70	1.89	1.89	1.90						
Rest	3.64	3.65	3.66	1.58	1.58	1.59						

765
 766
 767

768 **Extended Data Table 4| Estimated parameters for the homogenous model.**
 769 Estimates generated from model fit to the national datasets are in the grey shaded
 770 rows. The remaining rows provide the region-specific estimates. Best parameter
 771 estimates are presented as a bold median bounded by the lower and upper ends for the
 772 95% credible interval. Model runs are initiated on the day (t_0) when reported cases
 773 surpassed 1 in 5 million individuals: Belgium (day 1); England (day 29); Portugal
 774 (day 3); Spain (day 8).
 775

Country/Region	R_0			$1 - d_{max}$			t_0^d		
Belgium	3.298	3.301	3.310	0.208	0.209	0.210	16.299	16.354	16.357
Flanders	3.235	3.239	3.308	0.208	0.212	0.213	16.324	17.039	17.064
Rest	3.235	3.238	3.307						
Portugal	2.900	2.910	2.914	0.242	0.243	0.244	20.551	20.622	20.693
North/Centre	3.542	3.578	3.608	0.343	0.345	0.348	7.514	7.725	7.999
Rest	4.274	4.321	4.361						
Spain	3.028	3.031	3.034	0.149	0.150	0.150	28.329	28.360	28.393
Madrid	4.113	4.116	4.120	0.111	0.111	0.112	20.000	20.000	20.000
Catalunya	4.208	4.214	4.218						
Rest	3.735	3.751	3.752						
England	2.434	2.435	2.437	0.355	0.355	0.356	55.047	55.070	55.074
London	2.307	2.308	2.310						
NorthWest	2.602	2.603	2.604						
SouthEast	2.368	2.370	2.371						
Rest	2.502	2.503	2.504	0.359	0.360	0.360	54.577	54.578	54.578

776
 777
 778

779 **Extended Data Table 5| Model selection criteria.** Displays the maximum
 780 Loglikelihood obtained for each combination of model and data partitioning for each
 781 country, as well as the Akaike information criterion. Models are labelled by a sort
 782 name as follows: homog (homogenous); hetsus (heterogeneity in susceptibility);
 783 hetcon (heterogeneity in connectivity with constant CV); hetdyn (heterogeneity in
 784 connectivity with dynamic CV).
 785

<i>Country</i>	<i>Model</i>	<i>LL</i>	<i>AIC</i>
<i>Aggregate Data</i>			
<i>Portugal</i>	homog	2.25E+05	-4.50E+05
	hetsus	2.30E+05	-4.59E+05
	hetcon	2.30E+05	-4.60E+05
	hetdyn	2.30E+05	-4.59E+05
<i>Spain</i>	homog	1.77E+06	-3.54E+06
	hetsus	1.79E+06	-3.59E+06
	hetcon	1.79E+06	-3.58E+06
	hetdyn	1.79E+06	-3.58E+06
<i>England</i>	homog	1.67E+06	-3.33E+06
	hetsus	1.68E+06	-3.36E+06
	hetcon	1.68E+06	-3.36E+06
	hetdyn	1.68E+06	-3.36E+06
<i>Belgium</i>	homog	3.30E+05	-6.60E+05
	hetsus	3.33E+05	-6.66E+05
	hetcon	3.33E+05	-6.65E+05
	hetdyn	3.33E+05	-6.66E+05
<i>Regional Data</i>			
<i>Portugal</i>	homog	3.36E+05	-6.73E+05
	hetsus	3.55E+05	-7.11E+05
	hetcon	3.55E+05	-7.10E+05
	hetdyn	3.55E+05	-7.11E+05
<i>Spain</i>	homog	1.87E+06	-3.75E+06
	hetsus	1.96E+06	-3.91E+06
	hetcon	1.96E+06	-3.91E+06
	hetdyn	1.47E+06	-2.95E+06
<i>England</i>	homog	2.59E+06	-5.18E+06
	hetsus	2.63E+06	-5.25E+06
	hetcon	2.62E+06	-5.25E+06
	hetdyn	2.62E+06	-5.25E+06
<i>Belgium</i>	homog	3.74E+05	-7.48E+05
	hetsus	3.78E+05	-7.56E+05
	hetcon	3.78E+05	-7.55E+05
	hetdyn	3.78E+05	-7.55E+05

786